PROCEEDINGS OF SPIE

SPIEDigitalLibrary.org/conference-proceedings-of-spie

Millimeter-wave multistatic imaging system using software-defined radios for advanced multiplexing

Weite Zhang, Yi Huang, Juan Heredia-Juesas, Jose Martinez-Lorenzo

Weite Zhang, Yi Huang, Juan Heredia-Juesas, Jose A. Martinez-Lorenzo, "Millimeter-wave multistatic imaging system using software-defined radios for advanced multiplexing," Proc. SPIE 12111, Passive and Active Millimeter-Wave Imaging XXV, 1211106 (3 June 2022); doi: 10.1117/12.2616698

SPIE.

Event: SPIE Defense + Commercial Sensing, 2022, Orlando, Florida, United States

Downloaded From: https://www.spiedigitallibrary.org/conference-proceedings-of-spie on 17 Aug 2022 Terms of Use: https://www.spiedigitallibrary.org/terms-of-use

Millimeter-wave multistatic imaging system using software-defined radios for advanced multiplexing

Weite Zhang[a], Yi Huang[a], Juan Heredia-Juesas[a,b], and Jose A. Martinez-Lorenzo[a,b]

[a]Department of Electrical and Computer Engineering, Northeastern University, Boston, MA 02115, USA
[b]Department of Mechanical and Industrial Engineering, Northeastern University, Boston, MA 02115, USA

ABSTRACT

Millimeter-wave (mm-wave) multiple-in-multiple-out (MIMO) imaging systems have been explored to use more and more complicated radar waveforms to achieve advanced multiplexing and high-performance imaging. As the complexity of radar waveforms increases, conventional radars inevitably suffer from higher design difficulty and cost. This work presents a software-defined mm-wave (SDMMW) multistatic radar design by making use of cost-effective commercial software-defined radios (SDRs) and additional radio-frequency/mm-wave modules. Due to the great baseband flexibility of the SDRs, the efficient space-time-coded (STC) orthogonal frequency-division multiplexing (OFDM) is developed as the radar waveform to achieve simultaneous MIMO transmission at the same time and frequency. The radar is designed at 83.5 GHz with a frequency bandwidth of 4.8 GHz, where an 8-by-8 waveguide array is specially designed to form 64 virtual channels with a small element-separation of 9 mm for three-dimensional imaging applications. To further enhance the sensing capacity and improve the imaging resolution of the SDMMW radar, the spatial coding created by the compressive reflector antenna is combined with the efficient multiplexing based on the STC OFDM. Preliminary experimental results show good imaging performance, giving great potential for developing future high-performance mm-wave imaging systems with advanced multiplexing.

Keywords: Advanced multiplexing, compressive reflector antenna, multiple-in-multiple-out radar, multi-static, millimeter-wave, orthogonal frequency-division multiplexing, software-defined, space-time coding, three-dimensional imaging.

1. INTRODUCTION

Millimeter-wave (mm-wave) multiple-in-multiple-out (MIMO) imaging systems have been using multiplexing by either time-division,[1] or frequency-division,[2] or the combination of both.[3,4] Such multiplexing schemes can only enable one transmitter at the same time and frequency. Thus, more advanced multiplexing is desired for high-performance mm-wave imaging. One way is to use space-time coding (STC)[5] for simultaneous MIMO operation, which can achieve a higher receiving signal-to-noise ratio (SNR). Another way is to use orthogonal frequency-division multiplexing (OFDM)[6] to increase the spectral efficiency of imaging systems where more measurement samples per frequency bandwidth are obtained. Nonetheless, such advanced multiplexing always requires complicated radar waveform processing, which makes conventional mm-wave imaging systems suffer from high design complexity and cost, especially when the MIMO size is large.

Software-defined radio (SDR) is a general radio frequency (RF) transceiver which can perform traditional hardware functionalities, such as upconvertion/downconvertion, filtering, modulation/demodulation, by means of software.[7] With the help of the great flexibility afforded by software, software-defined mm-wave (SDMMW)

Further author information: (Send correspondence to W. Z.)
W. Z.: E-mail: zhang.weit@northeastern.edu
Y. H.: E-mail: huang.yi1@northeastern.edu
J. H.: E-mail: j.herediajuesas@northeastern.edu
J. A. M.: E-mail: j.martinez-lorenzo@northeastern.edu

Passive and Active Millimeter-Wave Imaging XXV, edited by David A. Wikner, Duncan A. Robertson, Proc. of SPIE Vol. 12111, 1211106
© 2022 SPIE · 0277-786X · doi: 10.1117/12.2616698

Downloaded From: https://www.spiedigitallibrary.org/conference-proceedings-of-spie on 17 Aug 2022
Terms of Use: https://www.spiedigitallibrary.org/terms-of-use

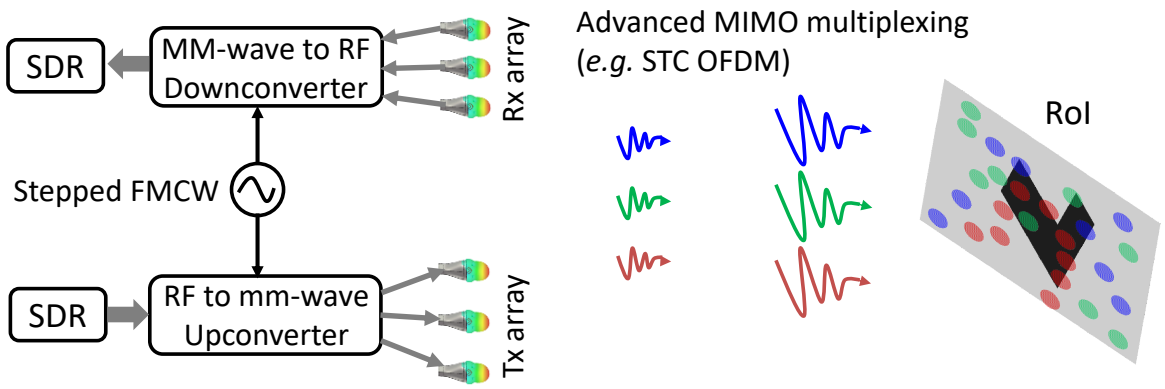

Figure 1. System concept of the software-defined millimeter-wave (SDMMW) multistatic radar. SDR: software-defined radio. Tx: transmitter. Rx: receiver. STC: space-time coding. OFDM: orthogonal frequency-division multiplexing. RoI: region of interest. FMCW: frequency-modulated continuous-wave.

radars are being developed to achieve advanced multiplexing. For instance, a 77-GHz single-channel SDMMW radar is integrated on the printed circuit boards for two-dimensional (2-D) range-Doppler measurements,[8] where an OFDM waveform with a bandwidth of 200 MHz is used. Another integrated 77-GHz SDMMW range-Doppler radar with a 4×4 multistatic array is designed,[9] which uses the code-division-based frequency-modulated continuous-wave (FMCW) with a chirp bandwidth of 250 MHz, where simultaneous MIMO operation is feasible.

SDMMW radars can also be implemented using cost-effective commercial SDRs, where additional RF/mm-wave modules are required for the RF-to-mm-wave or the mm-wave-to-RF conversions. Note such modularized radar designs outperform the integrated ones in terms of the cost and design period. As an example, a modularized SDMMW radar is designed at 28 GHz,[10] which consists of two identical 64-element phased arrays with one connected to the transmitting channel and the other one connected to the receiving channel. The wide bandwidth measurement over 1 GHz is implemented by stitching multiple OFDM waveforms at different local oscillator (LO) frequencies, each OFDM waveform having a bandwidth of 100 MHz. Note that the use of phased arrays is not optimal since phased arrays suffer from much higher hardware design complexity and cost, compared to multistatic arrays. Specifically, to achieve an equivalent number of virtual MIMO channels, the number of physical antennas in a phased array ($N \times M$ transceivers) will be much larger than that in a multistatic array (N transmitters + M receivers), especially when N and M are large.

This paper presents a SDMMW radar design in a multistatic setup, by leveraging commercial cost-effective SDRs and a modularized mm-wave MIMO front-end. The radar operates at 83.5 GHz with a frequency bandwidth of 4.8 GHz. The MIMO front-end consists of an 8-by-8 multistatic array, forming total 64 measurement channels for 3-D imaging applications. The virtual MIMO aperture has a square shape with a uniform element separation of 9 mm. The advanced multiplexing is implemented by the STC OFDM, where the STC is designed based on the Hadamard matrix[11,12] which allows simple decoupling and decoding for imaging processing. The first 3-D imaging experiment is carried out to image an array of corner reflectors.[13] To further improve the imaging resolution, the STC OFDM is combined with the spatial coding created by the compressive reflector antenna (CRA),[4,14] where the CRA increases the measurement diversity for a higher sensing capacity. Thus, the second 3-D imaging experiment is performed to image an L-shaped object. Preliminary experimental results show good imaging performance, giving great potential for developing future high-performance mm-wave imaging systems with advanced multiplexing.

2. SDMMW RADAR PROTOTYPE DESIGN

2.1 Hardware Subsystem

Figure 1 shows the general architecture of the SDMMW multistatic radar which consists of a multistatic array, multiple SDRs at both the transmitter (Tx) and receiver (Rx) ends, the RF-to-mm-wave upconverters in the Tx chains, and the mm-wave-to-RF downconverters in the Rx chain. In this work, the radar prototype is designed

Downloaded From: https://www.spiedigitallibrary.org/conference-proceedings-of-spie on 17 Aug 2022
Terms of Use: https://www.spiedigitallibrary.org/terms-of-use

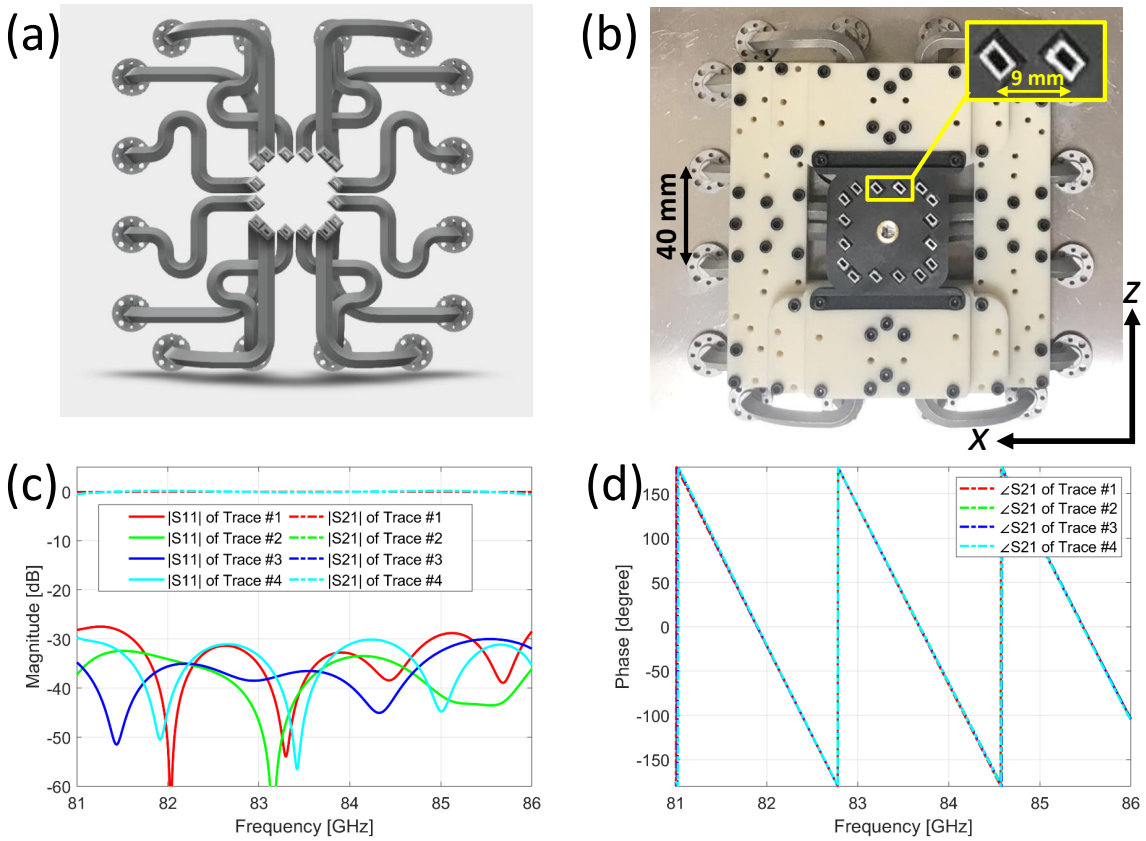

Figure 2. (a) is the simulated model of the waveguide bend array. (b) is the fabricated waveguide bend by the direct metal laser sintering (DMLS). (c) is the simulated magnitude responses of the four independent traces of the waveguide bend array. (d) is the simulated phase responses of the four independent traces of the waveguide bend array.

with a 8-by-8 multistatic array which is 3-D printed by the direct metal laser sintering (DMLS) to form 64 synthetic measurement channels. The radar is also equipped with 8 commercial cost-effective SDRs. Each SDR has two Tx-Rx channels, where one Tx-Rx channel is working in the loopback mode to estimate and compensate initial phase difference between the two RF carriers in the Tx chain and the Rx chain, respectively. The other Tx-Rx channel is for the raw data measurement for the 3-D object imaging. Each upconverter/downconverter are modularized by using one 90° RF coupler, two 180° RF couplers, and one mm-wave Tx/Rx mixer. An external tunable LO with a 16-way power splitter generates the coherent stepped FMCW for all the Tx and Rx channels. A synchronized clock module provides the clock references (10 MHz) and the timing references (1 PPS, pulse per second) for all associated hardware modules. The SDRs are attached to a USB 3.0 interface connected to a host personal computer (PC).

Note that the original Tx and Rx WR-12 ports of the mm-wave mixers are arranged in a square shape with an inter-port separation of 40 mm. Such a large separation is imposed by the physical dimension of the mm-wave mixer modules. To minimize the inter-port separation and reduce the sidelobe effect, a waveguide bend array is modeled and simulated, as shown in Figure 2(a). The fabricated waveguide bend array is given in Figure 2(b) where the UG-387/U flanges are to be connected to the WR-12 ports of the mm-wave mixers. The whole waveguide array consists of 8 Tx ports and 8 Rx ports, which are aligned along the $x-$ and z-axis, respectively, with an inter-port separation of 9 mm. To show the effectiveness of the waveguide array, full-wave simulations are performed on 4 of total 16 waveguide bends, which have mutually independent waveguide traces. Figures 2(c) and 2(d) show the simulated magnitude and phase responses, respectively. As we can see, the magnitude responses show the return losses $|S_{11}| < -25$ dB and the propagation losses $|S_{21}| \approx 0$ dB. The phase responses converge to the same phase patten for all the four waveguide bends, which is important for coherent MIMO

Downloaded From: https://www.spiedigitallibrary.org/conference-proceedings-of-spie on 17 Aug 2022
Terms of Use: https://www.spiedigitallibrary.org/terms-of-use

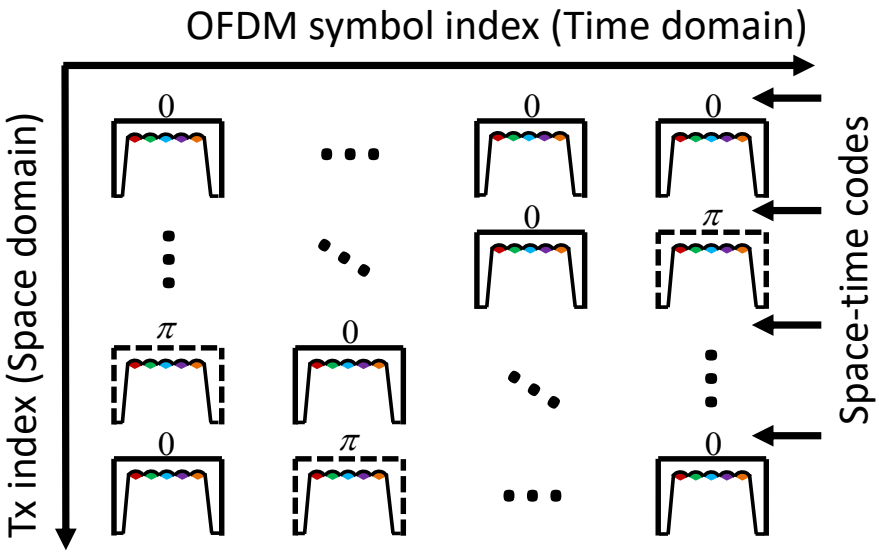

Figure 3. The STC OFDM waveform for the simultaneous MIMO operation where the i-th Tx transmits an sequence of OFDM symbols with the space-time codes (0 or π in phase, or -1 or $+1$ in magnitude). Each Rx will receive a waveform that is a coupled and delayed combination of the simultaneously transmitted STC OFDM symbols.

operation in imaging applications.

The baseband AD/DA sampling rate of the SDRs is 8 MS/s, resulting in an overall Tx/Rx data rate of 512 MB/s, namely 8 MS/s $\times$ 8 Bytes per complex float sample $\times$ 8 channels, approaching the maximum throughput of a typical USB 3.0 interface. The IF input/output at the SDRs is 700 MHz. The stepped FMCW sweeps from 13.4 GHz to 14.2 GHz with total $N_{\mathrm{c}} = 100$ equally-spaced frequencies. The Tx (or Rx) mm-wave mixer functions as a $\times 6$ multiplier and an upconverter (or a downconverter). Thus, the mm-wave operates at a center frequency of 83.5 GHz with a bandwidth of 4.8 GHz. The FMCW frequency step time is 500 μs where the dwell-time is $T_{\mathrm{d}} = 400$ μs that is necessary for a stable phase lock loop in the LO module, and the remaining $T_{\mathrm{a}} = 100$ μs is the maximum time period allowed for simultaneously transmitting and receiving the STC OFDM waveform.

2.2 Software Subsystem

Although the arbitrary waveform generation is possible by the SDRs, the radar prototype is designed to use the STC OFDM for the simultaneous MIMO transmission at the same time and frequency, which is a promising waveform to achieve a high spectral efficiency and a high receiving SNR. Note that although the STC OFDM has been widely used in 4G/5G wireless communications, it has not been explored in mm-wave imaging with a large MIMO size.[15] In this work, the space-time codes are specifically constructed based on the Hadamard matrix,[11,12] allowing simple decoupling and decoding for imaging processing. Figure 3 depicts the general concept of the STC OFDM for the MIMO operation where the i-th Tx transmits an sequence of OFDM symbols with the space-time codes, $-1/+1$ in magnitude (or $\pi/0$ in phase). Note the total number of Txs N_{t} needs to be the same as the number of Rxs or OFDM symbols. Also, the baseband STC OFDM is designed to have 32 subcarriers, $N_{\mathrm{subc}} = 32$. Thus, each Rx receives the coupled and delayed combination of the simultaneously transmitted STC OFDM symbols from different Txs, giving rise to the following forward model in the frequency domain,

$$\mathbf{R} = \mathbf{C}\mathbf{H} + \mathbf{n} \tag{1}$$

where $\mathbf{C}$ is the channel response that is to be estimated for the image reconstruction, $\mathbf{H}$ is the transmitted Hadamard matrix which is known at the receiver end, and $\mathbf{R}$ is the raw measurement at the receiver end with additive thermal noise $\mathbf{n}$. Thus, the channel response $\mathbf{C}$ can be estimated based on the inherent property of the

Downloaded From: https://www.spiedigitallibrary.org/conference-proceedings-of-spie on 17 Aug 2022
Terms of Use: https://www.spiedigitallibrary.org/terms-of-use

Hadamard matrix, namely

$$\begin{aligned}\mathbf{C} &= \mathbf{R}\mathbf{H}^{-1} \\ &= \frac{1}{N_t}\mathbf{R}\mathbf{H}^{\mathrm{T}}\end{aligned} \tag{2}$$

where $(\cdot)^{-1}$ is the matrix reversion, and $(\cdot)^{\mathrm{T}}$ is the matrix transpose. Note that each element of $\mathbf{C}$ corresponds to the transfer function of one Tx-Rx pair, which will be used to construct the measurement vector $\mathbf{g}$ for the imaging processing where either the pre-computed sensing matrix[3,16] or the inverse fast multipole method[17] can be used.

In addition to the STC OFDM waveform design, the software of the radar prototype runs in Python 2.0[18] with the customized application programming interface (API) functions which are to coordinate all the hardware modules for 3D imaging applications. In the software execution, the SDRs are initialized by 1) synchronizing the time registers of all the SDRs to 0 at the arrival of the first PPS edge; 2) generating and saving the baseband STC OFDM waveform samples for each Tx in the random-access memory (RAM) of the host PC; and 3) pre-loading the sensing matrices in the RAM, which will be used in the 3D imaging reconstruction. After the initialization, all the MIMO channels will wait for the measurement trigger at the next arrival of the PPS. The measurement trigger interval needs to be matched with the FMCW sweeping rate that is $N_{\mathrm{c}} \times (T_{\mathrm{d}} + T_{\mathrm{a}}) = 50$ ms per cycle. Thus, the measurement trigger interval should be $N \times 50$ ms, N being any positive integer, where the first 50 ms is for the radar waveform streaming and the following $(N-1) \times 50$ is the time period for the image formation. In the experiment, the host PC uses the i7-9750H processor with total 12 threads, where the averaged imaging processing time is ∼340 ms. Thus, to allow sufficient time for imaging processing, $N = 10$ is selected, corresponding to an overall image formation rate of 2 frames per second (fps).

The system parameters of the radar prototype are summarized in Table 1 where N_{t} is the number of Txs, N_{r} is the number of Rxs, N_{c} is the number of FMCW frequencies, N_{subc} is the number of OFDM subcarriers, Δd is the output inter-port separation, D_0 is the MIMO aperture dimension, BW is the radar frequency bandwidth, f_{c} is the center frequency of the mm-wave, T_{d} is the dwell-time at each FMCW frequency step, and T_{a} is for the time period for the STC OFDM waveform streaming.

Table 1. System design parameters of the radar prototype

Name	Value	Name	Value
N_{t}	8	Δd	9 mm
N_{r}	8	f_{c}	83.5 GHz
N_{c}	100	BW	4.8 GHz
N_{subc}	32	T_{d}	400 μs
D_0	36 mm	T_{a}	100 μs

3. THREE-DIMENSIONAL IMAGING EXPERIMENTS

3.1 Calibration Procedure

The radar system calibration is required before imaging any objects, which is to measure and compensate the phase and magnitude errors of all the measurement channels to ensure the coherent MIMO operation. In this experiment, a commercial corner reflector (Eravant SAJ-014-S1) with an edge length of 35.56 mm is used as the calibrator, which is placed at the near-field or the far-field of the MIMO aperture and facing the array center. In this case, the corner reflector is placed 150 cm away in front of the MIMO array. The calibration process can be described as

$$\tilde{\mathbf{g}} = (\mathbf{g} - \mathbf{g}_{\mathrm{BG}}) \cdot \left(\frac{\mathbf{g}_{\mathrm{C-SIM}}}{\mathbf{g}_{\mathrm{C-EXP}} - \mathbf{g}_{\mathrm{BG}}} \right) \tag{3}$$

Downloaded From: https://www.spiedigitallibrary.org/conference-proceedings-of-spie on 17 Aug 2022
Terms of Use: https://www.spiedigitallibrary.org/terms-of-use

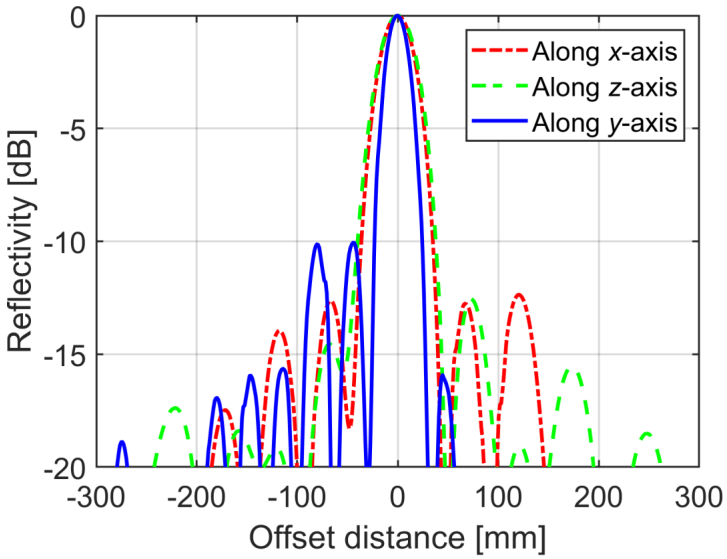

Figure 4. The measured point spreading functions along the cross-range (x-axis), elevation (z-axis), and range (y-axis), respectively, where the 3-dB beamwidths are 58.3 mm, 63.2 mm, and 38.4 mm, respectively.

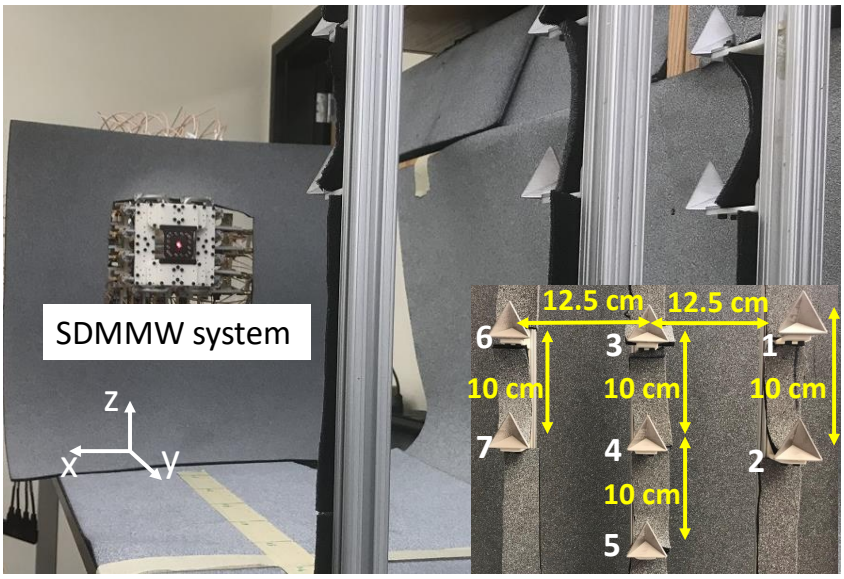

Figure 5. SDMMW imaging experiment to detect an array of corner reflectors.

where $\mathbf{g}_{\mathrm{BG}}$ is the background measurement in the absence of any object; $\mathbf{g}_{\mathrm{C-EXP}}$ is the measured response of the calibrator at the far-field of the MIMO aperture; $\mathbf{g}_{\mathrm{C-SIM}}$ is the simulated response of the same calibrator; $(\cdot/\cdot)$ is the element-wise division to measure the phase and magnitude errors for all MIMO channels at each frequency; $\mathbf{g}$ is the raw measurement vector before the calibration; and $\tilde{\mathbf{g}}$ is the calibrated measurement vector for the 3-D image formation.

3.2 3-D Imaging Results

The point spreading function (PSF) of the radar prototype is evaluated in order to see the focusing performance of the MIMO array after the calibration process. Figure 4 shows the measured PSFs along the cross-range (x-axis), elevation (z-axis), and range (y-axis), respectively, where the corresponding 3-dB beamwidths are 58.3 mm, 63.2 mm, and 38.4 mm, respectively.

Downloaded From: https://www.spiedigitallibrary.org/conference-proceedings-of-spie on 17 Aug 2022
Terms of Use: https://www.spiedigitallibrary.org/terms-of-use

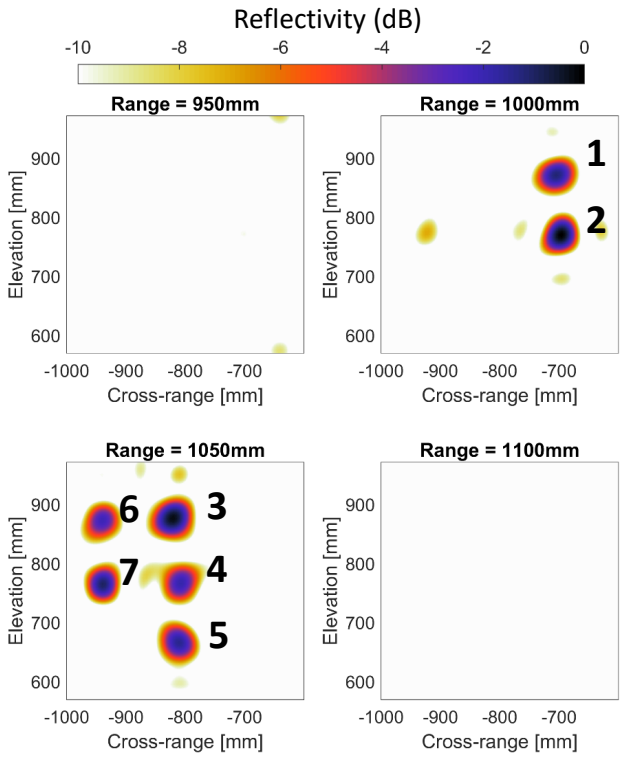

Figure 6. Experimental 3D imaging on the corner reflector array.

The experimental setup to image an array of corner reflectors is given in Figure 5, where the corner reflectors are customized and fabricated by the metal printing. The corner reflectors have an identical shape with an edge length of 36 mm. As we can see in the inserted subplot of Figure 5, the corner reflectors have a measured cross-range separation of 12.5 cm and an elevation separation of 10 cm. Additionally, the corner reflectors #1 and #2 are located at the range 100 cm; while the corner reflectors #3 − #7 are placed at the range 105 cm. The 3-D imaging results of the corner reflector array are plotted in Figure 6 where the object reflectivity is plotted at different range planes. As can be seen from the experimental imaging results, all the corner reflectors are well-imaged and distinguished from each other in 3-D, showing a good imaging performance achieved by the established radar prototype.

To further enhance the imaging resolution of the SDMMW multistatic system, the spatial[14,19] and/or spectral[20,21] coding over an aperture between the MIMO array and the imaging domain can be adopted, where a higher sensing capacity (or better imaging performance) can be obtained. In this work, the advanced multiplexing of the STC OFDM is further combined with the spatial coding created by the CRA. Note that the general CRA design and CRA imaging setup can be referred in our related works.[4,14] This paper mainly focuses on the feasibility study of using the CRA-based spatial coding in the SDMMW multistatic imaging system to enhance the sensing capacity. As a result, Figure 7(a) shows the physical dimensions of the L-shaped object under detection, and Figures 7(b)-7(d) show the corresponding object profile imaged at different range cuts, where a good match between the imaged object profile and the ground truth mesh is achieved.

4. CONCLUSION AND FUTURE WORK

This paper presents a new SDMMW multistatic radar system with efficient multiplexing for 3-D imaging applications. The radar prototype is designed by making use of cost-effective commercial SDRs. Due to the great baseband flexibility of the SDRs, the efficient radar waveform based on the STC OFDM is developed to achieve simultaneous MIMO transmission at the same time and frequency. The radar is designed at 83.5 GHz with a

Downloaded From: https://www.spiedigitallibrary.org/conference-proceedings-of-spie on 17 Aug 2022
Terms of Use: https://www.spiedigitallibrary.org/terms-of-use

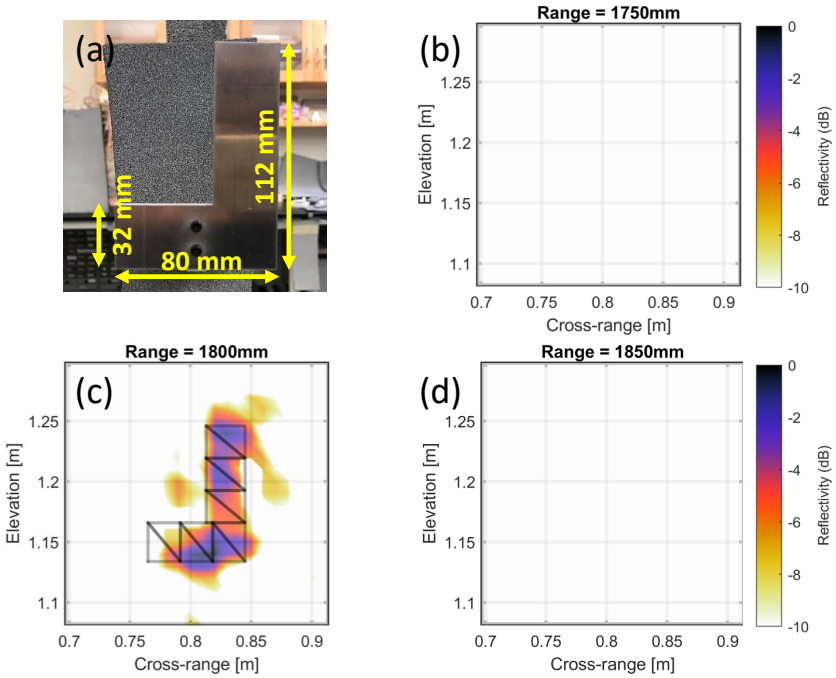

Figure 7. Experimental imaging results on the L-shaped metallic object by using the STC OFDM with the spatial coding of the CRA. (a) shows the dimensions of the L-shaped object, and (b)-(d) show the imaged object profile at different range cuts.

frequency bandwidth of 4.8 GHz, where an 8-by-8 waveguide array is specially designed to form 64 measurement channels with a small element-separation of 9 mm. To further enhance the imaging resolution of the SDMMW radar, the spatial coding created by the CRA is combined with the efficient multiplexing based on the STC OFDM. Preliminary experimental results show good imaging performance, giving great potential for developing future high-performance mm-wave radars with advanced multiplexing.

ACKNOWLEDGMENTS

This work was supported in part by the NSF CAREER Program under Award 1653671 and in part by the U.S. Department of Homeland Security under Award 2013-ST-061-ED0001.

REFERENCES

[1] Bleh, D., Rosch, M., Kuri, M., Dyck, A., Tessmann, A., Leuther, A., Wagner, S., Weismann-Thaden, B., Stulz, H.-P., Zink, M., Rieble, M., Sommer, R., Wilcke, J., Schlechtweg, M., Yang, B., and Ambacher, O., "*W* -band time-domain multiplexing fmcw mimo radar for far-field 3-d imaging," *IEEE Transactions on Microwave Theory and Techniques* **65**(9), 3474–3484 (2017).

[2] Schindler, D., Schweizer, B., Knill, C., Hasch, J., and Waldschmidt, C., "Mimo-ofdm radar using a linear frequency modulated carrier to reduce sampling requirements," *IEEE Transactions on Microwave Theory and Techniques* **66**(7), 3511–3520 (2018).

[3] Tirado, L. E., Zhang, W., Bisulco, A., Gomez-Sousa, H., and Martinez-Lorenzo, J. A., "Towards three-dimensional millimeter-wave radar imaging of on-the-move targets," in [*2018 IEEE International Symposium on Antennas and Propagation USNC/URSI National Radio Science Meeting*], 1959–1960 (2018).

[4] Zhang, W., Molaei, A., Heredia-Juesas, J., Tirado, L., Graham, K., Bisulco, A., Gomez-Sousa, H., and Martinez-Lorenzo, J. A., "Experimental results of a 3-d millimeter-wave compressive reflector antenna imaging system," *IEEE Antennas and Wireless Propagation Letters* **18**(1), 24–28 (2019).

Downloaded From: https://www.spiedigitallibrary.org/conference-proceedings-of-spie on 17 Aug 2022
Terms of Use: https://www.spiedigitallibrary.org/terms-of-use

[5] Santra, A., Ganis, A. R., Mietzner, J., and Ziegler, V., "Ambiguity function and imaging performance of coded fmcw waveforms with fast 4d receiver processing in mimo radar," *Digital Signal Processing* **97**, 102618 (2020).

[6] Knill, C., Roos, F., Schweizer, B., Schindler, D., and Waldschmidt, C., "Random multiplexing for an mimo-ofdm radar with compressed sensing-based reconstruction," *IEEE Microwave and Wireless Components Letters* **29**(4), 300–302 (2019).

[7] Jondral, F. K., "Software-defined radio–basics and evolution to cognitive radio," *EURASIP journal on wireless communications and networking* **2005**(3), 1–9 (2005).

[8] Pfeffer, C., Jahn, M., Feger, R., Huttner, R., and Stelzer, A., "A software defined radar platform for mm-wave sensing applications," in [*2014 11th European Radar Conference*], 281–284 (2014).

[9] Haderer, H., Feger, R., Pfeffer, C., and Stelzer, A., "Millimeter-wave phase-coded cw mimo radar using zero- and low-correlation-zone sequence sets," *IEEE Transactions on Microwave Theory and Techniques* **64**(12), 4312–4323 (2016).

[10] Guan, J., Paidimarri, A., Valdes-Garcia, A., and Sadhu, B., "3-d imaging using millimeter-wave 5g signal reflections," *IEEE Transactions on Microwave Theory and Techniques* **69**(6), 2936–2948 (2021).

[11] Damen, M. O., Abed-Meraim, K., and Belfiore, J.-C., "Diagonal algebraic space-time block codes," *IEEE Transactions on Information Theory* **48**(3), 628–636 (2002).

[12] Bolcskei, H., "Mimo-ofdm wireless systems: basics, perspectives, and challenges," *IEEE Wireless Communications* **13**(4), 31–37 (2006).

[13] Zhang, W., Huang, Y., Heredia-Juesas, J., and Martinez-Lorenzo, J. A., "Software-defined millimeter-wave multistatic radar with space-time-coded orthogonal frequency-division multiplexing," *IEEE Transactions on Microwave Theory and Techniques* **70**, 1620–1629 (Mar. 2022).

[14] Martinez Lorenzo, J. A., Heredia Juesas, J., and Blackwell, W., "A single-transceiver compressive reflector antenna for high-sensing-capacity imaging," *IEEE Antennas and Wireless Propagation Letters* **15**, 968–971 (2016).

[15] Schindler, D., Schweizer, B., Knill, C., Hasch, J., and Waldschmidt, C., "Synthetization of virtual transmit antennas for mimo ofdm radar by space-time coding," *IEEE Transactions on Aerospace and Electronic Systems* **57**(3), 1964–1971 (2021).

[16] Heredia-Juesas, J., Molaei, A., Tirado, L., Blackwell, W., and Martinez-Lorenzo, J. A., "Norm-1 regularized consensus-based admm for imaging with a compressive antenna," *IEEE Antennas and Wireless Propagation Letters* **16**, 2362–2365 (Jun. 2017).

[17] Alvarez, Y., Martinez-Lorenzo, J. A., Las-Heras, F., and Rappaport, C. M., "An inverse fast multipole method for geometry reconstruction using scattered field information," *IEEE Transactions on Antennas and Propagation* **60**, 3351–3360 (May 2012).

[18] Lutz, M., [*Programming python*], " O'Reilly Media, Inc." (2001).

[19] Molaei, A., Heredia-Juesas, J., Tirado, L., Zhang, W., Bisulco, A., Zhu, A., Cachay, D., Dagheyan, A. G., and Martinez-Lorenzo, J., "3d printed compressive horn antenna for high-sensing-capacity millimeter-wave imaging," in [*12th European Conference on Antennas and Propagation (EuCAP 2018)*], 1–4 (Apr. 2018).

[20] Hunt, J., Gollub, J., Driscoll, T., Lipworth, G., Mrozack, A., Reynolds, M. S., Brady, D. J., and Smith, D. R., "Metamaterial microwave holographic imaging system," *J. Opt. Soc. Am. A* **31**, 2109–2119 (Oct 2014).

[21] Sleasman, T. A., Imani, M. F., Diebold, A. V., Boyarsky, M., Trofatter, K. P., and Smith, D. R., "Implementation and characterization of a two-dimensional printed circuit dynamic metasurface aperture for computational microwave imaging," *IEEE Transactions on Antennas and Propagation* **69**, 2151–2164 (Apr. 2021).

Downloaded From: https://www.spiedigitallibrary.org/conference-proceedings-of-spie on 17 Aug 2022
Terms of Use: https://www.spiedigitallibrary.org/terms-of-use